American Mineralogist, Volume 97, pages 739–749, 2012

Petedunnite ($CaZnSi_2O_6$): Stability and phase relations in the system CaO-ZnO-SiO_2

Alexandra L. Huber,[1,*] Soraya Heuss-Aßbichler,[1] Karl Thomas Fehr,[1] and Geoffrey D. Bromiley[2,3]

[1]Department für Geo- und Umweltwissenschaften, Ludwig-Maximilians Universität, Theresienstrasse 41, D-80333 München, Germany
[2]Bayerisches Geoinstitut Universität Bayreuth, Universitätsstrasse 30, D-95447 Bayreuth, Germany
[3]School of GeoSciences, The University of Edinburgh, Grant Institute, The King's Buildings, West Main Road, Edinburgh EH9 3JW, U.K.

Abstract

The phase relations of petedunnite [$CaZnSi_2O_6$ (pd)] were determined experimentally at *P*-*T* conditions up to 2.5 GPa and 1100 °C. Single-phase petedunnite is formed at high pressures ($P > 0.8$ GPa). Reversed experiments show that at lower pressures and temperatures >650 °C petedunnite decomposes to willemite [Zn_2SiO_4 (wil)], hardystonite [$Ca_2ZnSi_2O_7$ (har)], and quartz [SiO_2 (qtz)] according to the reaction 4 pd = wil + 2 har + 3 qtz. The boundary curve for this equilibrium reaction is given by P (GPa) = –0.093 (0.029) + 0.0014 (0.0003) T (°C), by disregarding the phase transition of quartz. The stability field of wil + har + qtz is restricted toward lower temperatures by zinc-feldspar [$CaZnSi_3O_8$ (zfsp)] according to the known reaction: wil + 2 har + 7 qtz = 4 zfsp. These reactions intersect at 650(1) °C/0.78(0.01) GPa, generating an invariant point I_{pd}. Additionally, petedunnite-breakdown reaction is intersected by the low/high-quartz phase transition curve, generating an invariant point I^{pd}_{qtz} at ~840 °C, 1.04 GPa. At temperatures <650 °C, further reactions occur in the system CaO-ZnO-SiO_2 including the doubly degenerate reaction zfsp = pd + qtz and 3 pd = har + wil + zfsp, which also intersect the invariant point I_{pd}. All reactions involving petedunnite display shallow positive slopes within the *P*/*T*-field, indicating that the crystallization of petedunnite is highly pressure sensitive over a wide temperature range. This means that an increasing petedunnite component in pyroxene shifts its stability field to higher pressures, similar to the effect of a jadeitic component.

The study of natural clinopyroxene and the correlation of its zinc content with published *P*-*T* conditions of these mineral assemblages confirmed a significant relationship between extraordinary high-zinc concentrations in pyroxene and high-metamorphic pressure conditions. In addition, the petedunnite component is obviously sensitive to the prevailing fluid conditions in terms of the fugacity ratio f_{S_2}/f_{O_2}. Furthermore, a distinct temperature dependency of the zinc component was observed in the range of trace element concentration. In consequence, Zn turns out to be a key element with regard to its implementation as a sophisticated petrogenetic indicator of metamorphic conditions. Therefore, routine measurement of zinc in element analyses of clinopyroxenes is strongly recommended.

Keywords: Zinc, clinopyroxene, petedunnite, stability, phase relations, skarn, petrogenetic indicator, geobarometry, experimental calibration

Introduction

Zinc usually occurs as a trace element in silicates. High-zinc contents in silicates have been observed in artificial systems, such as bottom ashes and blast furnace slag (e.g., Förstner and Hirschmann 1997; Ettler et al. 2001). Clinopyroxene, as a major constituent of metallurgical slag, may contain up to 3.1 wt% ZnO (Ettler et al. 2001) or even up to 7.5 and 7.8 wt% ZnO, respectively (Lottermoser 2002; Puziewicz et al. 2007). In nature, the host rocks of metamorphic zinc deposits contain clinopyroxenes with elevated zinc contents. In skarn deposits, the zinc content of clinopyroxene is discussed as an indicator for petrogenetic processes. In a detailed study, Nakano et al. (1991, 1994) demonstrated that the zinc content in clinopyroxenes correlates significantly with the type of skarn deposit. They observed average Zn concentrations ranging from 50 to >1000 ppm. Shimizu and Iiyama (1982) reported clinopyroxenes from the Pb-Zn Nakatatsu skarn mine, coexisting with ore, which contained 1000–10 000 ppm Zn. Heuss-Aßbichler and Fehr (1994) recorded hedenbergitic clinopyroxene with up to 9000 ppm Zn in a phase assemblage with sphalerite from a Pb-Zn skarn (Åmmeberg, Sweden). Clinopyroxenes showing remarkably high-Zn concentrations (3.3 to 12.6 wt%) were collected in the Franklin area of New Jersey, U.S.A. (Frondel and Ito 1966; Essene and Peacor 1987). Based on these zinc-rich clinopyroxenes, the end-member petedunnite ($CaZnSi_2O_6$) was first described by Essene and Peacor (1987). Corresponding to their distribution in composition space, they assumed a complete solid solution between petedunnite and hedenbergite-johannsenite-diopside [$Ca(Fe,Mn,Mg)Si_2O_6$].

* E-mail: ahuber@min.uni-muenchen.de

0003-004X/12/0004–739$05.00/DOI: http://dx.doi.org/10.2138/am.2012.3836

Only a limited number of experimental studies have been performed on the petedunnite-bearing clinopyroxene solid-solution series. Crystal chemistry and thermodynamic properties of synthetic petedunnite-hedenbergite [$Ca(Zn,Fe)Si_2O_6$] solid-solution series were investigated by Heuer et al. (2005, 2002a, 2002b), Huber et al. (2004), and Huber and Fehr (2003). Ohashi et al. (1996) refined the crystal structures of the petedunnite-jervisite [$(NaCa)(Sc,Zn)Si_2O_6$] solid-solution series. These petedunnite-bearing clinopyroxenes were synthesized at high pressure and temperature conditions (6 GPa, 1197–1297 °C, 20–30 h). Up to now, however, the stability field of end-member petedunnite was largely unknown. Overall, experimental investigations on silicate systems containing ZnO are scarce. Olesch et al. (1982) and Doroshev et al. (1983) studied the subsolidus phase relations along the join ZnO-SiO_2. They determined, experimentally, the stability field of zinc clinopyroxene ($ZnSiO_3$) up to 10 GPa. Toward lower pressures (2.85 GPa/1200 °C), $ZnSiO_3$ breaks down to the phase assemblage willemite (Zn_2SiO_4) + quartz. Morimoto et al. (1975) and Arlt and Angel (2000) investigated the structure of $ZnSiO_3$-pyroxene. Three different $ZnSiO_3$ modifications are distinguished, including two distinct $ZnSiO_3$-clinopyroxene polymorphs (space group $C2/c$) and $ZnSiO_3$-pyroxene (space group $P2_1c$) (Arlt and Angel 2000). Correspondingly, with increasing pressure, they observed two phase transitions. Segnit (1954) performed experiments in the system CaO-ZnO-SiO_2 at temperatures between 1164 and 1590 °C at 1 atm. He determined the relation of solid phases, like willemite (Zn_2SiO_4), hardystonite ($Ca_2ZnSi_2O_7$), tridymite, and various calcium silicates in equilibrium with the liquid phase. In this system, Fehr and Huber (2001) discovered zinc-feldspar ($CaZnSi_3O_8$) as a new ternary phase. Zinc-feldspar is the reaction product of willemite + hardystonite + quartz. It is stable at low-pressure and -temperature conditions (Fehr and Huber 2001). Essene and Peacor (1987) synthesized petedunnite in the system CaO-ZnO-SiO_2. Preliminary high-pressure experiments at 900 °C, 2.0 GPa with an experiment duration of 6 days yielded single-phase petedunnite. Huber et al. (2004) confirmed these synthesis conditions by synthesizing single-phase petedunnite at 1000 °C, 2.0 GPa over 69 h. Petedunnite synthesis conditions at higher pressures (6 GPa, 1197 °C, 20 h) were reported by Nestola et al. (2010). They studied the high-pressure behavior of petedunnite crystal structure at pressures up to 8.23 GPa.

The purpose of the present study is (1) to experimentally determine the stability field of end-member petedunnite $CaZnSi_2O_6$ and (2) to elucidate the phase relations of petedunnite $CaZnSi_2O_6$ in the system CaO-ZnO-SiO_2 (Fig. 1). This forms part of a long-term study to understand the miscibility of petedunnite with hedenbergite-johannsenite-diopside solid solutions and to highlight the role of Zn as a petrographic indicator in skarn deposits.

Experimental methods

Experiments were conducted using pure, annealed crystalline phases prepared from sources of reagent grade SiO_2 (99.995%), $CaCO_3$ (99.999%), and ZnO (99.99%). To perform the synthesis experiments, stoichiometric mixtures were prepared according to the bulk composition of petedunnite $CaZnSi_2O_6$ (initial mixtures A, B) and zinc-feldspar $CaZnSi_3O_8$ (initial mixture C) (Table 1). After homogenization, starting mixture A was divided into two aliquots [A(1) and A(2)]. Starting mixtures A(1) and C were decarbonized at 900 °C, 1 atm for 36 h. Mixture A(2) was sintered at 500 °C, 1 atm for 36 h to perform synthesis experiments in the presence of a CO_2 vapor phase. Starting mixture B was prepared by mixing and annealing appropriate proportions of SiO_2 and $CaCO_3$ at 900 °C, 1 atm for 12 h. After decarbonazing, ZnO was added to the mixture. After preparation, all starting mixtures were characterized by means of X-ray powder diffraction. Mixture A(1) and C crystallized to willemite, hardystonite, and quartz; mixture A(2) contained additionally zinc-feldspar and calcite. Mixture B was composed of wollastonite, quartz, and zincite in various amounts.

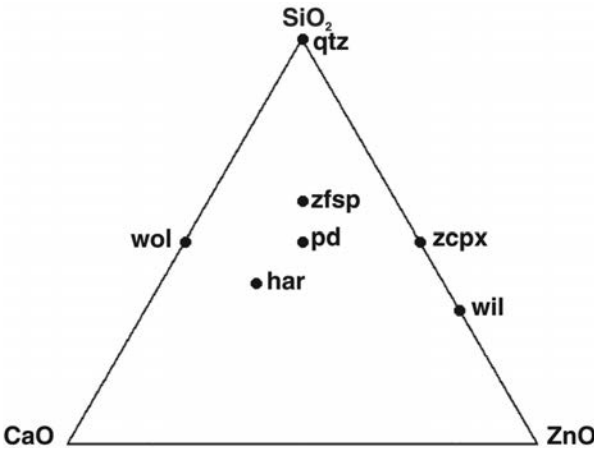

Figure 1. Projection of ternary and binary phases in the system CaO-ZnO-SiO_2 (in mol%). Abbreviations are wollastonite (wol), willemite (wil), zinc-clinopyroxene (zcpx), hardystonite (har), petedunnite (pd), and zinc-feldspar (zfsp).

Synthesis experiments were conducted over the pressure range 1 atm to 2.5 GPa and in the presence of a free hydrous phase (Table 1). Starting materials were sealed in platinum capsules with 10 wt% water. Experiments in the temperature range 750 to 900 °C at pressures of 0.2 to 0.5 GPa were conducted using an internally heated gas-media apparatus (Yoder 1950; Huckenholz et al. 1975). Temperature and pressure fluctuations were typically ±5 °C and ±0.002 GPa, respectively. Experimental methods used have been described elsewhere (Huckenholz et al. 1974; Sepp 1998). Experiments at pressures higher than 0.8 GPa were performed using a piston-cylinder solid-media apparatus. Most of the high-pressure experiments were performed with a low-friction NaCl-cell, designed by Fehr (1992), exhibiting friction as low as 1%. Temperature and pressure fluctuations were typically ±5 °C and ±0.002 GPa, respectively. Additional experiments (pb2, pb3, pgb2, pr15-pr19, pr21, pr213) were carried out at the Bayerisches Geoinstitut using an end-loaded piston-cylinder type apparatus. Experimental methods used here have been described elsewhere (Huber et al. 2004), with the exception that smaller, 3 mm long, welded platinum capsules (prepared from 2 mm diameter Pt tubing) were used and inserted into alumina sample holders. Talc-pyrex sample assemblies (0.5") were used with an internal, tapered, graphite resistance furnace. Temperature and pressure fluctuations were typically lower than ±1 °C and ±0.01 GPa, respectively. To determine the stability of petedunnite, reversed experiments were conducted with a stochiometric mixture of petedunnite [synthesized from starting material A(1), experiments pb2, pb3, p20 in Table 1], and willemite + hardystonite + quartz [synthesized from starting material A(1), experiments p4, p5, p11, p12 in Table 1] in appropriate amounts (mixture D in Table 1).

Run products were examined for homogeneity by means of oil immersion microscopy. For X-ray diffraction measurements, each sample was prepared on a low-background sample holder (silicon single-crystal section). The unit-cell parameter of petedunnite were recorded on a Seifert XRD3003, using a Cu X-ray tube (λ = 1.54056/1.54439 Å), operating at 40 kV and 35 mA. Intensity measurements were taken at room temperature in steps of 0.01° over 2θ ranges from 18 to 100° with a counting time of 30 s per step. Furthermore powder diffraction patterns were recorded on a Phillips PW 1729 diffractometer, using a Cu X-ray tube (λ = 1.54056/1.54439 Å), operating at 40 kV and 30 mA. Intensity measurements were taken at room temperature in steps of 0.02° over 2θ ranges from 5 to 70° with a counting time of 2 s per step. Silicon [a_0 = 5.43088(4) Å] or quartz [a_0 = 4.91344(4) Å, c_0 = 5.40524(8) Å] grains were used as internal standards. Experiments performed at the Bayerisches Geoinstitut were analyzed

TABLE 1. Experimental results of synthesis experiments and reversed experiments in the absence of a hydrous vapor phase at pressures >0.7 GPa and in the presence of a hydrous vapor phase at pressures ≤0.7 GPa

Exp.	P (GPa)	T (°C)	Time (days)	Initial*	Results†
Synthesis experiments					
pg1	2.5	1100	3	A(1)	pd + qtz + L
p25	2.0	600	12	A(1)	pd (har + qtz + wil)
p24	2.0	700	12	A(1)	pd (har + qtz + wil)
p21	2.0	800	5	A(1)	pd (har + qtz + wil)
p19	2.0	900	4	A(1)	pd (har + qtz + wil)
p20	2.0	900	6	A(1)	pd
pb2	2.0	970	4	A(1)	pd
pb3	2.0	970	4	A(1)	pd
p1	2.0	1000	3	A(1)	pd
p3	2.0	1000	5	A(1)	pd (har + qtz + wil)
p9	1.9	1000	3	A(1)	pd
p22	1.5	700	17	A(1)	pd (har + qtz + wil)
p15	1.5	900	3	A(1)	pd (har + qtz + wil)
pgb2	1.3	900	1	B	pd (har + qtz + wil)
p23	1.2	600	8	A(1)	pd (har + qtz + wil)
p17r†	1.0	800	3	A(1)	pd (har + qtz + wil)
p16	1.0	900	5	A(1)	har + qtz + wil
z11	0.7	720	11	C	har + qtz + wil
z16	0.7	750	4	C	har + qtz + wil
p18	0.5	750	13	A(1)	har + qtz + wil (zfsp)
p7	0.5	800	7	A(1)	har + qtz + wil (zfsp)
p14	0.5	825	7	A(1)	har + qtz + wil
z6	0.5	850	9	C	har + qtz + wil
h9	0.5	900	7	A(2)	har + qtz + wil (CO_2^v-H_2O^v)
p11	0.3	900	7	A(1)	har + qtz + wil
p12	0.2	870	7	A(1)	har + qtz + wil
z5	0.2	900	7	C	har + qtz + wil
z2	0.2	850	42	C	har + qtz + wil
p4	1 atm	930	15	A(1)	har + qtz + wil
p5	1 atm	930	15	A(1)	har + qtz + wil
z0	1 atm	950	3	C	har + qtz + wil
Reversed experiments on reaction 1					
pr16	1.6	975		D	pd grew
pr15	1.5	900		D	pd grew
pr18	1.3	975		D	pd grew
pr213	1.2	900		D	pd grew
pr1	1.2	800		D	pd grew
pr19	1.1	725		D	pd grew
pr8	1.1	900		D	har +qtz + wil grew
pr20	1.1	975		D	har + qtz + wil grew
pr5	1.0	900		D	har + qtz + wil grew
pr6	1.0	900		D	har + qtz + wil grew
pr17	0.9	725		D	pd grew
pr21	0.85	725		D	har + qtz + wil grew
pr2	0.8	800		D	har + qtz + wil grew

* A(1) = $CaZnSi_2O_6$ composition sintered at 900 °C/1 atm: willemite + hardystonite + quartz; A(2) = $CaZnSi_2O_6$ composition sintered at 500 °C/1 atm: zinc-feldspar + willemite + hardystonite + quartz + calcite; B = $CaZnSi_2O_6$ composition, SiO_2 and $CaCO_3$ sintered at 900 °C/1 atm: wollastonite + quartz + zincite; C = $CaZnSi_3O_8$ composition sintered at 900 °C/1 atm: willemite + hardystonite + quartz; D = stoichometric mixture for reversed experiments: equal amounts of petedunnite (experiments pb2, pb3, p20) and willemite + hardystonite + quartz (experiments p4, p5, p11, p12).

† Phases in parentheses: traces or less than 5 wt% of total run product; sole exception: p17r (pd: 15wt%, har + wil + qtz: 85%). Abbreviations: Petedunnite (pd), hardystonite (har), willemite (wil), quartz (qtz), liquid (L) CO_2^v-H_2O^v: CO_2-H_2O.

using a Siemens D-5000 diffractometer with a Cu X-ray tube, operating at 35 mA and 45 kV. Measurements were taken at steps of 0.02° over the same 2θ range of 5 to 70° with a counting time of 3–5 s per step.

Reversal brackets were examined by means of the principles of quantitative diffraction analysis. The theoretical background for this method was originally outlined by Alexander and Klug (1948) and Klug and Alexander (1974). Reaction progress proceeds proportional to the changing intensity ratio of single lines of petedunnite (pd) and hardystonite (har). It is given by the relation of the diffracted intensities $I^p_{pd,har} = [I^p_{pd(110)}/I^p_{har(111)}]$ from the run product (p) to the equivalent relation from the starting mixture (s) $I^s_{pd,har} = [I^s_{pd(110)}/I^s_{har(111)}]$. The ratio $I^p_{pd,har}/I^s_{pd,har}$ is used to determine the direction of the reaction. If

$I^p_{pd,har}/I^s_{pd,har} > 1$, petedunnite grew;
$I^p_{pd,har}/I^s_{pd,har} = 1$, no reaction occurred;
$I^p_{pd,har}/I^s_{pd,har} < 1$, hardystonite + quartz + willemite grew.

Using samples with small particle sizes (<10 μm), the mean relative error of the quantitative X-ray technique is in the range from 3 to 4% (e.g., Suryanarayanan 1989; Jahanbagloo and Zoltai 1968; Klug et al. 1948). The relative error σ for the relation $I^p_{Pd,Har}/I^s_{Pd,Har}$ increases to 6% according to the principles of error propagation formalism (e.g., Chatterjee 1991). The results are given in Table 2.

The electron microprobe (Camebax SX50) was operated at 15 kV acceleration voltage and 15 nA beam current. Synthetic wollastonite (Ca, Si) and sphalerite (Zn) were used as standards and a matrix correction was performed by the PAP procedure (Pouchou and Pichoir 1984). The reproducibility of standard analyses was >99% for each element routinely analyzed. As a trace element, Zn was detected at 25 kV acceleration voltages and 100 nA within 100 s per data point. At these measurement conditions possible interactions of crystals adjacent to zinc-minerals (e.g., sphalerite), were taken into account. According to our calculations, the size of the interaction volume at 25 kV would be not more than 5 μm^3. Avoiding overestimations, e.g., caused by high-voltage-induced excitement of from zinc-bearing minerals, the reproducibility of the data was >90%. San Carlos clinopyroxene (BY16) was used as a microprobe standard material. According to instrumental neutron activation analysis (INAA), it contains 76.7 ± 6.7 ppm Zn (Blum 1982). Trace element analysis of BY16 by microprobe yielded routinely 90 ± 20 ppm Zn. This is in good agreement with the data detected by INAA (Blum 1982).

RESULTS

Synthesis experiments demonstrate that petedunnite ($CaZnSi_2O_6$) as a single-phase can be synthesized at 900–1000 °C and 1.9–2.0 GPa (Table 1, experiments p20, pb2, pb3, p1, p3, p9). The best conditions to obtain single crystals of petedunnite from 1 to 25 μm in size were 970 °C, 2.0 GPa. At lower temperatures or lower pressures, small amounts of willemite, hardystonite, and quartz (5 wt% or less) were formed in addition to petedunnite, even in experiments with long experiment durations (e.g., experiments p24, p22 in Table 1). Electron microprobe analyses confirm that all petedunnite is stochiometric. Synthetic petedunnite predominantly forms euhedral crystals as shown in Figure 2. The crystals are colorless and have a vitreous luster. In contrast to the observations of Essene and Peacor (1987) on natural petedunnite, synthetic petedunnite shows a bright blue luminescence under the electron microprobe beam with a 15 kV acceleration voltage. X-ray reflection data from petedun-

TABLE 2. Relation of $I^p_{pd,har}/I^s_{pd,har}$ of the diffracted intensities $I^p_{pd,har} = [I^p_{pd(110)}/I^p_{har(111)}]$ from the run product to the equivalent relation from the starting mixture $I^s_{pd,har} = [I^s_{pd(110)}/I^s_{har(111)}]$

Exp.	$I^p_{pd,har}/I^s_{pd,har}$	Results
pr213	284.73	pd grew
pr1	163.68	pd grew
pr15	54.16	pd grew
pr16	12.91	pd grew
pr18	5.46	pd grew
pr19	1.77	pd grew
pr17	1.38	pd grew
pr20	0.50	har + qtz + wil grew
pr8	0.46	har + qtz + wil grew
pr21	0.29	har + qtz + wil grew
pr5	0.28	har + qtz + wil grew
pr6	0.10	har + qtz + wil grew
pr2	0.05	har + qtz + wil grew

Note: If $I^p_{pd,har}/I^s_{pd,har} > 1$, pd grew ; if $I^p_{pd,har}/I^s_{pd,har} = 1$, no reaction occurred; and if $I^p_{pd,har}/I^s_{pd,har} < 1$ har + qtz + wil grew; $\sigma(I^p_{pd,har}/I^s_{pd,har}) = 6\%$.

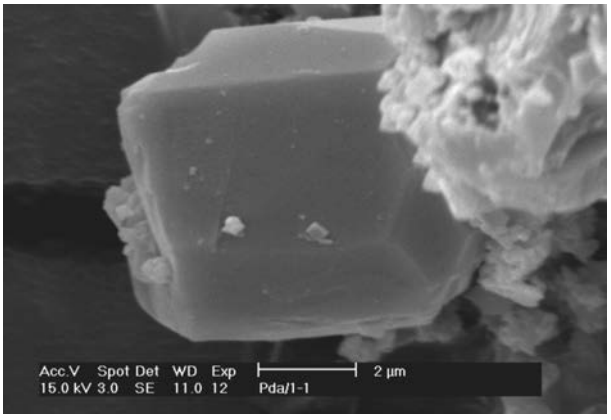

FIGURE 2. SEM photograph of a single petedunnite crystal, grown at 1000 °C, 2.0 GPa (see Table 1, experiment p1).

nite (experiment p3, Table 1) were used to refine a monoclinic unit cell with parameters of a = 9.8044(8), b = 8.9764(8), c = 5.2493(4) Å, β = 105.77(4)°, unit-cell volume (V^{uc}) = 444.6 Å^3. The space group is $C2/c$, and with Z = 4 the molar volume (V^{mol}) is 66.93 cm^3/mol. The unit-cell parameters correspond very well with values reported for synthetic $CaZnSi_2O_6$ by Essene and Peacor (1987): a = 9.803(6), b = 8.975(7), c = 5.243(7) Å, β = 105.75(7)°, V^{uc} = 444(2) Å^3. Our data are also in very good agreement with Nestola et al. (2010). They determined unit-cell parameters of synthetic petedunnite by means of single-crystal X-ray diffraction: a = 9.8055(2), b = 8.9778(3), c = 5.2499(1) Å, β = 105.763(3)°, V^{uc} = 444.78(2) Å^3.

At high temperatures, a melt-bearing assemblage was observed. Starting from petedunnite bulk composition at 1100 °C (2.5 GPa) and dry reaction conditions, a liquid phase was determined additionally to petedunnite + quartz (Table 1, experiment pg1). Toward lower pressures, the stability field of petedunnite is bounded by the reaction:

4 petedunnite = willemite + 2 hardystonite + 3 quartz. (1)

Correspondingly, synthesis experiments conducted over the P-T range 725–975 °C and 1 atm to 1.1 GPa lie within the stability field of willemite + hardystonite + quartz. This phase assemblage was synthesized from oxide mixes with both petedunnite and zinc feldspar bulk compositions (starting materials A and C, Table 1). Reaction 1 was bracketed by reversed experiments between 725–975 °C and 0.8–1.3 GPa (experiments pr1, pr2, pr5, pr6, pr8, pr15-pr21, and pr213 in Table 1). Reaction 1 has a flat positive slope in P-T space. This is consistent with the nucleation of petedunnite from crystalline starting mixtures at 800 °C, 1.0 GPa (experiment p17r in Table 1). The P-T conditions for this experiment lie very close to the phase boundary, which explains why the assemblage petedunnite + (hardystonite + willemite + quartz) was noted after a experiment duration of 3 days. Over the P-T range investigated, the influence of the low-high quartz phase transition must also to be considered. Within the stability field of low-quartz, reaction 1 ends at an invariant point I^{pd}_{qtz} projected on the low-high quartz phase transition (Mirwald and Massonne 1980) ~840 °C, 1.04 GPa (see Fig. 3). Consequently, at the invariant point the slope of reaction 1 changes slightly. Due to the phase transition, the difference of reaction volume (ΔV_r) is only 3.09 cm^3/mol. Hence, the slope-alteration is smaller than the precision of the error bar. Correspondingly, over the P-T range of interest, the decomposition reaction(s) of petedunnite can be adequately fitted to a single straight-line. Thus, reaction 1 can be described by P (GPa) = –0.093 (0.029) + 0.0014 (0.0003) T (°C) if one disregards the high-low quartz phase transition.

ZINC CONTENTS IN NATURAL CLINOPYROXENES

Data on Zn contents of natural clinopyroxenes are scarce, as zinc is usually not routinely analyzed. The Zn contents of clinopyroxenes from skarn deposits were analyzed by electron microprobe in this study in a reconnaissance fashion. The locations of these clinopyroxenes are given in Table 3. The samples are from skarn deposits, calc-silicate, peridotite, and granulite. All clinopyroxenes are members of the hedenbergite-diopside solid-solution series. Additionally some pyroxenes exhibit a fassaite component [$Ca(Mg,Al)(Si,Al)_2O_6$] (samples fass2, TU-12, TU-49, and by16) or an aegirine component ($NaFe^{3+}Si_2O_6$) (sample gs-7). Minor components are johannsenite ($CaMn^{2+}Si_2O_6$) (samples fe-1, fe-2, gs-7, and gs-9) and jadeite ($NaAlSi_2O_6$) (samples TU-49 and by16). The average zinc content in clinopyroxenes varies from 50 to 4980 ppm. The highest zinc contents were found in pyroxenes that were in contact with sphalerite (Zn,Fe)S. The electron microprobe compositional map of sample gs-9 from Åmmeberg (Sweden) depicts the distribution of zinc in garnet and clinopyroxene adjacent to sphalerite (Fig. 4). In this sample, high-zinc contents (up to 8800 ppm) were detected in clinopyroxene, as well as in garnet (up to 7000 ppm). A clinopyroxene sample from Franklin, New Jersey, U.S.A., shows up to 7980 ppm Zn (sample TU-49).

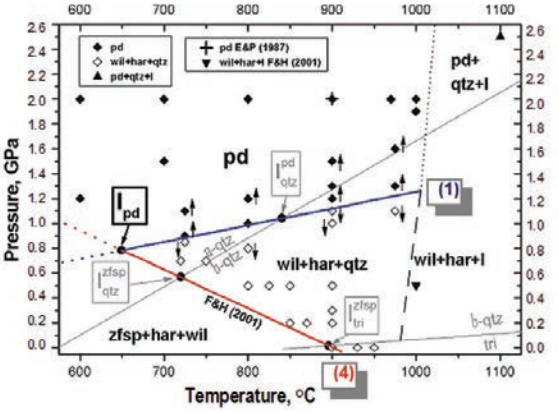

FIGURE 3. Pressure vs. temperature plot of data on $CaZnSi_2O_6$ composition obtained for reaction 1: 4 petedunnite = willemite + 2 hardystonite + 3 quartz. Symbols: open diamonds, willemite + hardystonite + quartz; filled diamonds, petedunnite; upward triangle, petedunnite + quartz + liquid; downward triangle, willemite + hardystonite + liquid. The arrows denote the direction of reversed experiments on reaction 1. I^{pd}_{qtz} is the five-phase invariant point of petedunnite + willemite + hardystonite + low-quartz + high-quartz. The data for the high-low quartz transition are taken from Mirwald and Massonne (1980). The location of reaction 4: 4 zinc-feldspar = willemite + 2 hardystonite + 7 quartz is given according to Fehr and Huber (2001). Error bars are within symbol size. (Color online.)

DISCUSSION

The experimental results clearly show that single-phase petedunnite ($CaZnSi_2O_6$) is formed at high pressures ($P > 0.8$ GPa). At lower pressures, petedunnite decomposes to willemite (Zn_2SiO_4), hardystonite ($Ca_2ZnSi_2O_7$), and quartz (SiO_2) according to reaction 1 (see Fig. 3). Based on their preliminary investigation, Rothkopf et al. (1998) implied a shallow negative slope for reaction 1. However, the results of this study, which were obtained by reversed experiments, prove a shallow positive slope for this reaction. By disregarding the phase transitions of quartz, the boundary curve for this equilibrium reaction is given by P (GPa) = –0.093 (0.029) + 0.0014 (0.0003) T (°C). Additionally, a synthesis experiment (performed at 800 °C/1.0 GPa) confirms the phase boundary. Our data are in good agreement with previous studies in which petedunnite was synthesized. Essene and Peacor (1987) synthesized petedunnite at 900 °C/2.0 GPa. Synthesis experiments performed by Huber et al. (2004) yielded petedunnite at 1000 °C/2.0 GPa. Segnit (1954) and Fehr and Huber (2001) performed synthesis experiments at pressure conditions below the stability boundary of petedunnite. Segnit (1954) observed the phase assemblage willemite, hardystonite, and tridymite at 1164 °C/1 atm. The results of this study were confirmed by the data of Fehr and Huber (2001). They observed the phase assemblage willemite, hardystonite, and quartz at pressures ≤1.0 GPa and high temperatures (≥720 °C) due to the decomposition of zinc-feldspar ($CaZnSi_3O_8$).

The stability of petedunnite is restricted at higher tempera-

TABLE 3. Locations and sources of natural zinc-bearing clinopyroxenes

Sample	Location	Rock type	Reference
fe-1	El Hammam, Central Morocco	skarn	Sonnet and Verkaeren (1989)
fe-3	Dartmoor, Red-A-ven Mine, Cornwall, Great Britain	skarn	Peng Qiming and Bromley (1992)
fass2	Monzoni, Italy	calc-silicate	Ferry et al. (2002)
bb1a	Breitenbrunn, Grube Fortuna, Erzgebirge, Germany	skarn	Galilaeer (1967)
bb1b	Breitenbrunn, Grube Fortuna, Erzgebirge, Germany	skarn	Galilaeer (1967)
bb4	Breitenbrunn, Grube St. Christoph, Erzgebirge, Germany	skarn	Galilaeer (1967)
bb5	Breitenbrunn, Grube Fortuna, Erzgebirge, Germany	skarn	Galilaeer (1967)
at-1	Breitenbrunn, Grube unverhofftes Glück an der Achte Antonsthal, Erzgebirge, Germany	skarn	Galilaeer (1967)
gs-7	Långban, Sweden	skarn	Jonsson and Broman (2002)
gs-9	Åmmeberg, Sweden	skarn	Billström (1991), Kumpulainen et al. (1996)
gs-16	King Island, Australia	skarn	Wesolowski and Ohmoto (1988)
TU-12	Arendal, Norway	skarn	Olmi et al. (2000)
TU-49	Franklin, New Jersey, U.S.A.	granulite	Johnson and Skinner (2003)
by16	San Carlos, Arizona, U.S.A.	peridotite	Yu and Smith (1983)

Note: All clinopyroxenes are members of the hedenbergite-diopside solid-solution series.

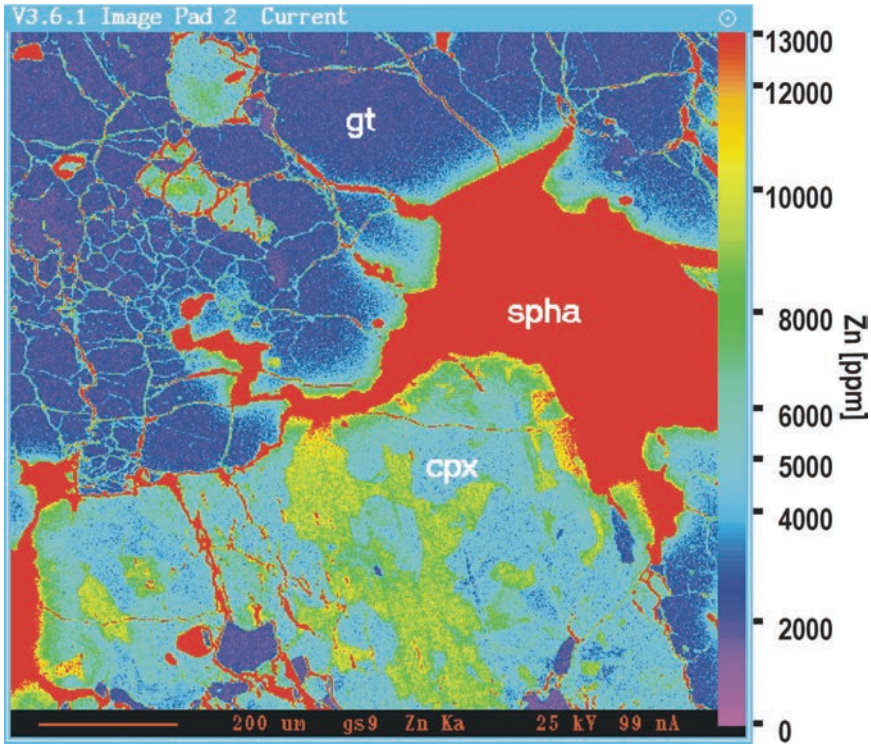

FIGURE 4. Electron microprobe compositional map, with respect to Zn, showing clinopyroxene in a phase assemblage with garnet and sphalerite. Diffusion zones are apparent in the clinopyroxene and garnet with Zn-enrichment and iron depletion. Up to 8800 ppm of zinc was detected in this clinopyroxene from Åmmeberg (Sweden). (Color online.)

tures. Above 1000 °C (2.0 GPa), petedunnite decomposes under dry conditions to a melt-bearing assemblage. Synthesis experiments at 1100 °C (2.5 GPa) indicate the onset of partial melting and the stability of the phase assemblage petedunnite + quartz + liquid. Thus, a solidus curve can be drawn tentatively in the range 1.3 to 2.5 GPa, as shown in Figure 3. At lower pressures (0.5 GPa/1000 °C), Fehr and Huber (2001) observed a liquid-bearing assemblage for experiments with zinc-feldspar compositions. They depicted the stability field of willemite + hardystonite + quartz up to 900 °C. According to the results of this study, the stability field of willemite + hardystonite + quartz extends up to 975 °C (at 1.1 GPa). Consequently, the dry solidus line shifts toward higher temperatures, as Fehr and Huber (2001) predicted. The intersection of these two dry solidus lines with reaction 1 occurs at ~1000 °C/1.25 GPa (see Fig. 3).

At low temperatures, reaction kinetics are very sluggish. Therefore, the stability limit of petedunnite at $T < 650$ °C was derived based on the principles of chemographic analyses for the system CaO-ZnO-SiO_2. In addition to the phases that determine reaction 1, zinc-feldspar must also be taken into account and three additional reactions have to be considered

petedunnite + quartz = zinc-feldspar (2)
3 petedunnite = hardystonite + willemite + zinc-feldspar (3)
4 zinc-feldspar = willemite + 2 hardystonite + 7 quartz. (4)

Fehr and Huber (2001) determined the position of reaction 4 experimentally at low-pressure conditions ($P < 1.0$ GPa, T 600–900 °C). Reaction 4 displays a steep negative slope in the P-T field, as depicted in Figure 3. By disregarding the phase transitions of quartz, the slope of reaction 4 is given by P (GPa) = 2.797 (0.325) – 0.0031 (0.0004) T (°C) (Fehr and Huber 2001). Reaction 4 intersects reaction 1 at 650(1) °C/0.78(0.01) GPa and defines the position of the invariant point I_{pd}. Considering the SiO_2 phase transitions, further invariant points occur in the system CaO-ZnO-SiO_2. Reaction 1 is intersected by the low-high quartz phase transition. Based on the data of Mirwald and Massonne (1980), I^{pd}_{qtz} is expected at ~840 °C, 1.04 GPa. Reaction 4 is affected by the low-high quartz phase transition (I^{zfsp}_{qtz}) and the high quartz–tridymite phase transition (I^{zfsp}_{tri}). According to Fehr and Huber (2001) I^{zfsp}_{qtz} is generated at 720 °C/0.57 GPa and I^{zfsp}_{tri} at 896 °C/0.016 GPa.

There are no data available for reactions 2 and 3. According to the chemographic analysis, their metastable extensions must pass into the stability field of the assemblage hardystonite + willemite + quartz, as depicted in Figure 5. This restricts their positions to low temperatures. Correspondingly, the doubly degenerated reaction 2 restricts the stability field of zinc-feldspar toward higher pressures, and petedunnite and quartz are formed. Toward lower pressures, the stability field of petedunnite is bounded by reaction 3 and petedunnite decomposes to hardystonite, willemite, and zinc-feldspar. The P-T slopes of reactions 2 and 3 can be estimated by using the Clausius-Clapeyron equation [$dP/dT = \Delta S_r/\Delta V_r$] to the entropy and volume changes of the corresponding phase assemblages.

Thermodynamic data have been estimated for willemite (White and Roberts 1988) and hardystonite (Haussühl and Liebertz 2004), however no data are available for petedunnite and zinc-feldspar. Hence, to a first approximation, ΔV_r at standard conditions ($\Delta V^0_r = \Delta V^{1bar, 20\,°C}_r$) was calculated. The value of ΔV^0_r is strongly positive for both univariant reactions 2 and 3 (see Table 4). Thus, the sign of ΔS_r is the determining factor for the slopes of these reactions. One can distinguish between two main cases. In principle, a negative slope for reaction 2 ($\Delta S_r < 0$) is possible. It can vary from shallow to steep, without violating Schreinemaker's rules. Alternatively, if the slope of reaction 2 is positive ($\Delta S_r > 0$), reaction 3 must have a positive slope. In this case, reactions 2 and 3 must have extremely shallow slopes due to the position of their metastable extensions within the stability field of the assemblage hardystonite + willemite + quartz. Therefore, the crystallization of petedunnite (reactions 1 to 3) is pressure sensitive over a wide temperature range, as depicted in Figure 5. The latter constraint [$\Delta S_r^{(3)}/\Delta V_r^{(3)} > 0$] proves to be reasonable when one compares the system CaO-ZnO-SiO_2 with NaO-Al_2O_3-SiO_2. Reaction 2 is analogous to the reaction albite = jadeite + quartz, which also shows a positive P-T slope. In both systems, toward higher pressures, a phase with a similar feldspar structure (Fehr and Huber 2001) decomposes and pyroxene (space group $C2/c$) + quartz is formed. The positive slope of reaction 2 is shallower than that of albite-breakdown reaction, as depicted in Figure 6. The albite-breakdown reaction to jadeite and quartz provides the basis of an important geothermobarometer in many assemblages of the blueshist and the eclogite facies (e.g., Bucher and Frey 1994a). The equilibrium conditions of the petedunnite-breakdown reaction to zinc-feldspar and quartz are barely temperature dependent, which highlights its particular suitability for geobarometry. Analog to an increase in jadeitic component (Bucher and Frey 1994b), an increase in petedunnite component in pyroxene is expected to be associated with an increase pressure. Synthesis experiments performed by Huber and Fehr (2002, 2003) and Huber et al. (2004), demonstrated that the mineralization of zincian hedenbergite [Ca(Fe,Zn)

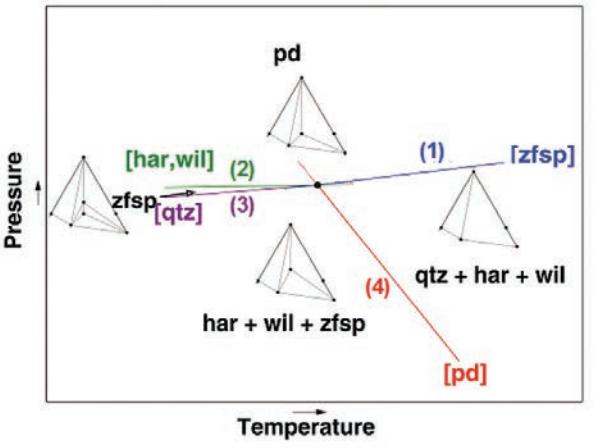

FIGURE 5. Chemographic relations between zinc-feldspar + willemite + hardystonite + quartz + petedunnite. Reactions: (1) 4 petedunnite = willemite + 2 hardystonite + 3 quartz [zfsp]; (2) petedunnite + quartz = zinc-feldspar [hard, wil]; (3) 3 petedunnite = hardystonite + willemite + zinc-feldspar [qtz]; (4) 4 zinc-feldspar = willemite + 2 hardystonite + 7 quartz [pd]. Phases in brackets denote that they are not involved in the reaction. Abbreviations are as shown in Figure 1. (Color online.)

TABLE 4. Slopes of reactions 2 and 3 in the system CaO-ZnO-SiO_2 within the *P-T*-field on the base of calculations according to the Clausius-Clapeyron equation, by assuming $\Delta S > 0$ and using ΔV_r at standard conditions ($\Delta V_r^0 = \Delta V_r^{1bar, 20\,°C}$) as a first approximation

Reaction	ΔV_r^0	d*P*/d*T*
(2) petedunnite + low-quartz = zinc-feldspar	113.94 cm³/mol	>0
(3) 3 petedunnite = hardystonite + willemite + zinc-feldspar	379.82 cm³/mol	>0

Si_2O_6] is pressure-controlled. The stability field of the synthetic petedunnite-hedenbergite [$Ca(Zn,Fe)Si_2O_6$] solid-solution series shifts toward higher pressures with an increase in the petedunnite component. Hence, if rocks are Zn-rich, clinopyroxene with a petedunnite component is expected to occur in medium- to high-pressure metamorphic terranes.

Few studies have shed light on petedunnite substitution in clinopyroxenes to understand metallogenic processes in different deposit types (e.g., Nakano 1998; Core et al. 2005). Zinc content in clinopyroxene was considered to be a function of temperature and fluid properties, however the role of pressure on the concentration of Zn in clinopyroxenes was suggested to be trivial (Nakano et al. 1991). Various samples from different zinc-deposits were analyzed to verify if the obtained experimental data on natural systems represent different metamorphic conditions (Tables 3 and 5). The majority of the clinopyroxenes analyzed display low to average zinc concentrations (<850 ppm) and were formed under low-pressure conditions (Galilaeer 1967; Wesolowski and Ohmoto 1988; Sonnet and Verkaeren 1989; Peng Qiming and Bromley 1992; Olmi et al. 2000). However, some clinopyroxenes have extraordinary high-zinc contents; the highest values (up to 5000 ppm on average) were detected in clinopyroxene from Pb-Zn skarn deposits in the Bergslagen region, Sweden (samples gs-9, gs-7, Tables 3 and 5). Remarkably high-zinc concentrations (up to 4300 ppm) were also detected in clinopyroxene from Franklin, New Jersey, U.S.A. (sample TU-49, Tables 3 and 5). Zinc accumulation models in these two deposits differ (e.g., Allen et al. 1996; Holtstam and Mansfeld

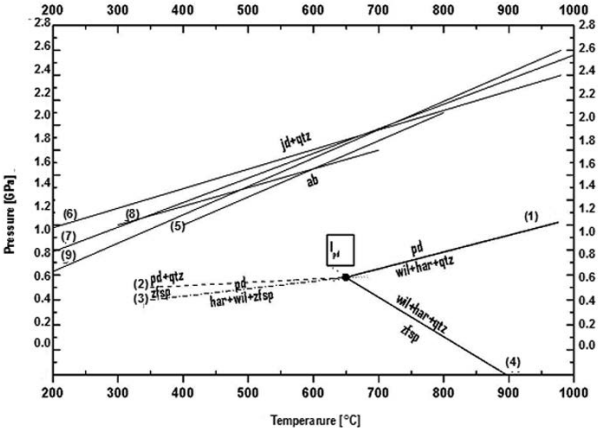

FIGURE 6. Pressure vs. temperature plot of data for reactions 1 to 4 (see Fig. 5) and for the reaction jadeite + quartz = albite from (5) Proyer (2003), (6) Newton and Kennedy (1968), (7) Birch and LeComte (1960), (8) Popp and Gilbert (1972), (9) Newton and Smith (1967).

2001; Volkert 2001; Johnson and Skinner 2003; Wagner et al. 2005). However, according to Johnson and Skinner (2003) Bergslagen appears to be the closest analog to Franklin. Both ore provinces experienced a series of metamorphic phases with different complex processes of overprinted metamorphic and deformational events (e.g., Allen et al. 1996; Johnson and Skinner 2003). Most notably, both also experienced high-pressure metamorphism. Both areas were affected by metamorphic peak conditions of > ~0.4 GPa and > ~600 °C (e.g., Jonsson and Broman 2002; Andersson et al. 2006; Peck et al. 2006) which is in good agreement with the results of this study. Accordingly, significant zinc enrichment in natural clinopyroxenes is associated with elevated pressures during mineralization processes.

Corresponding to the results of this study, zinc contents of clinopyroxenes formed in low-pressure terranes are in the range of trace element concentrations. Our data are in good agreement with Nakano et al. (1991, 1994) and Nakano (1998). Their detailed studies on geochemical systematics of skarn clinopyroxenes yielded average zinc concentrations ranging from 50 to >1000 ppm. They used the zinc content of skarn clinopyroxenes as a petrogenetic indicator to distinguish between various skarn types: low-zinc contents (mostly <200 ppm) occur in Fe-Cu skarn deposits and high values (mostly >200 ppm) occur in Pb-Zn skarn deposits. Our data from Arendal, Norway (Fe-Cu skarn deposit), and from Breitenbrunn, Germany (Pb-Zn skarn deposit), agree with this trend (see Fig. 7). For W-skarn deposits the characteristic threshold has been given at 500 ppm (Nakano et al. 1994; Nakano 1998). They found higher zinc contents only in clinopyroxenes from Sn-W-F skarn deposits. Our preliminary data from King Island, Australia (Cu-W-Mo skarn deposit), Dartmoor, Great Britain, and Rei Hammam, Morocco (Sn-W-F skarn deposits), differ from this classification, as more than 500 ppm Zn was observed in Cu-W-Mo skarn clinopyroxene. Hence, the Nakano classification can be extended by incorporation of our data (see Fig. 7). At Cornwall, Evans (1993) observed a zonal sequence of Fe, Pb-Zn, Cu, Sn skarn ore mineralization with decreasing distance from the intrusive body. Accordingly, reflecting this sequence, an increase in the zinc concentration in clinopyroxene correlates with increasing metamorphic temperatures.

Totally different mechanisms of zinc enrichment in clinopyroxene occur along the contact with zinc-ore. Figure 4 depicts a sample from the Åmmeberg Pb-Zn skarn deposit. The clinopyroxene shows up to 8800 ppm zinc (sample gs-9, Table 5). Analyses adjacent to sphalerite were not taken into account due to possible interaction of the electron beam. The high value corresponds to the observation of Shimizu and Iiyama (1982) who reported clinopyroxene analyses from the Nakatatsu skarn mine, coexisting with ore, which contained up to 10 000 ppm Zn. Both clinopyroxene and garnet adjacent to sphalerite exhibit zones with Zn-enrichment and iron depletion. Along the grain boundary with sphalerite, the clinopyroxene displays up to a 60 µm broad zone of zinc enrichment (Fig. 4). The reaction rim between clinopyroxene and sphalerite implies solid-state diffusion. This corresponds to the observation of Nakano (1998) and to the experimental results of Heuer et al. (1996). According to Nakano (1998), along the contact with skarn sphalerite, the width of the Zn enrichment zone in clinopyroxene is generally

TABLE 5. Representative electron microprobe analyses of clinopyroxenes

	fe-1*	sd[H]	fe-2*	sd[H]	fass2*	sd[H]	bb1a*	sd[H]	bb1b*	sd[H]
SiO_2	52.11	0.13	48.69	0.15	45.80	0.70	53.88	0.23	53.66	0.01
TiO_2	0.00	0.00	0.00	0.00	1.06	0.09	0.02	0.00	0.01	0.00
Al_2O_3	0.02	0.00	0.06	0.00	8.84	0.86	0.46	0.04	0.67	0.02
Fe_2O_3										
FeO	8.49	0.69	23.59	1.32	4.49	0.33	2.20	0.05	2.85	0.32
MnO	2.87	0.19	1.97	0.19	0.05	0.00	0.53	0.12	0.58	0.14
MgO	10.71	0.72	1.93	0.25	12.93	0.48	16.12	0.03	15.64	0.39
CaO	25.29	0.20	23.55	0.16	25.57	0.13	26.35	0.23	26.32	0.00
Na_2O	0.01	0.00	0.03	0.00	0.02	0.00	0.00	0.00	0.00	0.00
Cr_2O_3										
NiO										
sum	99.51	0.33	99.82	0.27	98.56	0.30	99.57	0.28	99.72	0.08
cations										
Si	1.990	0.005	1.982	0.006	1.707	0.024	1.977	0.016	1.972	0.004
Ti	0.000	0.000	0.000	0.000	0.030	0.002	0.001	0.000	0.001	0.000
Al	0.001	0.000	0.003	0.000	0.388	0.038	0.020	0.002	0.029	0.001
Fe^{3+}										
Fe^{2+}	0.271	0.022	0.803	0.045	0.134	0.010	0.068	0.002	0.088	0.011
Mn	0.093	0.006	0.068	0.006	0.002	0.000	0.017	0.004	0.018	0.004
Mg	0.610	0.041	0.117	0.015	0.718	0.026	0.882	0.004	0.857	0.020
Ca	1.035	0.008	1.027	0.007	1.021	0.004	1.036	0.006	1.036	0.001
Na	0.001	0.000	0.002	0.000	0.001	0.000	0.000	0.000	0.000	0.000
Cr										
Ni										
Zn (ppm)	140	60	260	90	50	10	190	60	430	40
up to max. Zn (ppm)	320		500		70		330		500	
	bb4*	sd[H]	bb5*	sd[H]	at-1*	sd[H]	gs-7*	sd[H]	gs-9*	sd[H]
SiO_2	52.88	0.13	54.29	0.16	54.66	0.04	54.42	0.16	50.36	0.23
TiO_2	0.00	0.00	0.00	0.00	0.02	0.00	0.00	0.00	0.03	0.00
Al_2O_3	0.28	0.03	0.45	0.06	0.60	0.07	0.12	0.02	0.17	0.04
Fe_2O_3										
FeO	10.10	0.83	3.57	0.10	3.43	0.49	15.41	1.15	16.43	0.39
MnO	0.82	0.11	0.65	0.03	0.27	0.07	2.55	0.04	1.64	0.16
MgO	11.78	0.59	15.66	0.17	15.28	0.63	7.48	0.76	6.12	0.41
CaO	25.27	0.20	26.05	0.15	25.19	0.42	13.75	1.24	24.05	0.24
Na_2O	0.03	0.00	0.00	0.00	0.34	0.03	5.27	0.49	0.04	0.02
Cr_2O_3										
NiO										
sum	101.16	0.12	100.66	0.17	99.78	0.21	98.97	0.03	98.82	0.11
cations										
Si	1.978	0.005	1.984	0.006	2.004	0.003	2.003	0.001	2.001	0.007
Ti	0.000	0.000	0.000	0.000	0.001	0.000	0.000	0.000	0.006	0.001
Al	0.009	0.001	0.014	0.002	0.026	0.004	0.006	0.001	0.008	0.002
Fe^{3+}							0.388	0.043	0.000	0.000
Fe^{2+}	0.316	0.036	0.109	0.003	0.106	0.015	0.005	0.001	0.546	0.014
Mn	0.026	0.004	0.020	0.001	0.009	0.002	0.084	0.010	0.055	0.005
Mg	0.657	0.043	0.853	0.009	0.837	0.030	0.434	0.042	0.362	0.022
Ca	1.013	0.008	1.020	0.006	0.992	0.012	0.574	0.050	1.024	0.007
Na	0.001	0.000	0.000	0.000	0.025	0.002	0.398	0.038	0.003	0.001
Cr										
Ni										
Zn (ppm)	510	180	210	80	600	200	3740	1080	4980	2300
up to max. Zn (ppm)	1050		390		800		5000		8800	
	Gs-16*	sd[H]	TU-12*	sd[H]	TU-49*	sd[H]	by16*	sd[H]		
SiO_2	52.85	0.19	48.00	0.26	46.63	0.28	51.45	0.51		
TiO_2	0.00	0.00	0.13	0.04	0.60	0.08	0.66	0.03		
Al_2O_3	0.37	0.09	6.80	0.28	5.45	0.38	7.51	0.14		
Fe_2O_3										
FeO	7.34	0.89	4.93	0.19	12.89	0.21	3.24	0.03		
MnO	0.78	0.19	0.28	0.03	2.10	0.09	0.10	0.00		
MgO	12.53	1.07	13.71	0.16	7.47	0.17	14.79	1.47		
CaO	25.22	0.17	25.26	0.15	21.46	0.14	19.76	0.36		
Na_2O	0.16	0.03	0.05	0.01	1.75	0.08	1.58	0.02		
Cr_2O_3							0.73	0.01		
NiO							0.04	0.00		
sum	99.25	0.32	99.16	0.20	98.34	0.16	99.86	0.11		
cations										
Si	1.997	0.007	1.816	0.010	1.864	0.011	1.863	0.018		
Ti	0.000	0.000	0.003	0.001	0.015	0.002	0.018	0.001		
Al	0.012	0.003	0.221	0.009	0.187	0.013	0.320	0.006		
Fe^{3+}										
Fe^{2+}	0.232	0.028	0.156	0.006	0.431	0.007	0.098	0.001		
Mn	0.025	0.006	0.009	0.001	0.071	0.003	0.003	0.000		
Mg	0.706	0.060	0.773	0.009	0.445	0.010	0.798	0.079		
Ca	1.021	0.007	1.024	0.006	0.919	0.006	0.767	0.014		

(continued on next page)

TABLE 5.—*CONTINUED*

	Gs-16*	sd[H]	TU-12*	sd[H]	TU-49*	sd[H]	by16*	sd[H]
Na	0.006	0.001	0.002	0.000	0.068	0.003	0.111	0.001
Cr							0.021	0.000
Ni							0.001	0.000
Zn (ppm)	850	130	270	70	4260	1090	90	20
up to max. Zn (ppm)	1070		660		7980		150	

* Samples, see Table 1. [H] = standard deviation (2σ).

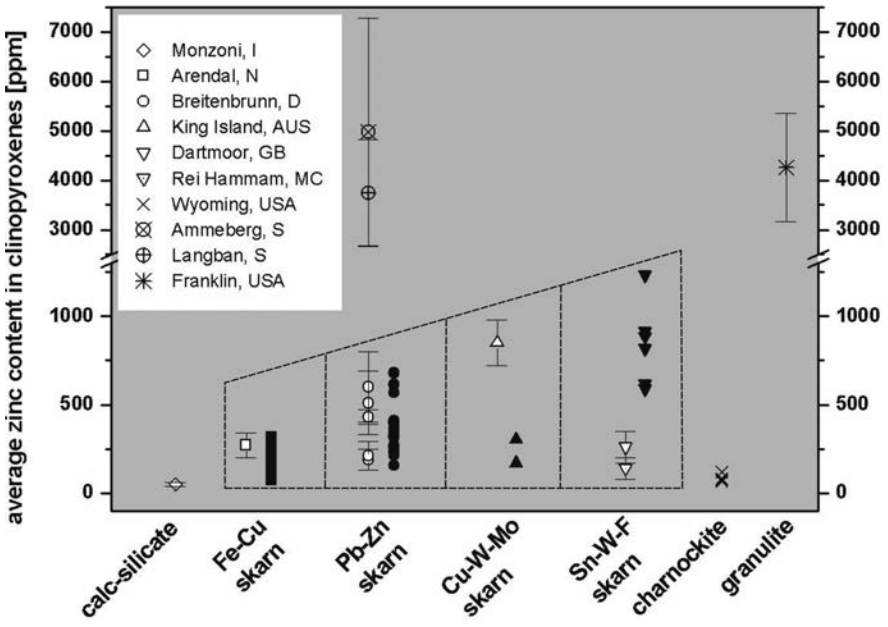

FIGURE 7. Mean zinc content in clinopyroxenes from charnockite (data from Frost et al. 2000), calc-silicate, granulite, and several skarn deposits (open signs); data from Japanese skarn deposits according to Nakano et al. (1991, 1994) (filled signs); classification of different skarn types according to Evans (1993) (dashed lines); for electron microprobe data, see Table 5.

around 100 µm. Preliminary experiments performed at defined O_2- and S_2-fugacities demonstrate grain-boundary diffusion between sphalerite and hedenbergitic clinopyroxene resulting from an intercrystalline exchange of Fe^{2+} for Zn^{2+} (Heuer et al. 1996). They observed up to 70 µm penetration depth of zinc in clinopyroxene adjacent to sphalerite under conditions controlled by the pyrrhotite-pyrite-magnetite buffer. There are indications, that the formation of a petedunnite component in clinopyroxene is favored by a relatively low f_{S_2}/f_{O_2} ratio (e.g., Essene and Peacor 1987; Heuer et al. 1996). Possible reactions involving oxygen and sulfur fugacities, which buffer the substitution of Zn into clinopyroxene silicate and oxide minerals, are reported by Essene and Peacor (1987), Huber et al. (2004), and Core et al. (2005).

In summary, various important applications result from the study of the zinc clinopyroxene petedunnite. Pure petedunnite shows a large stability field at high pressures. In terms of experimental petrology, the barely temperature dependent decomposition reaction 1 is very useful for experimental calibrations of high-pressure apparatus. Furthermore, the present results on pure petedunnite emphasize the suitability of zincian clinopyroxenes as sophisticated petrogenetic indicators for zinc-rich metamorphic rocks. High-pressure conditions during metamorphism are indicated by high-Zn contents in clinopyroxene due to the high-pressure stability of the end-member petedunnite; at low-pressure conditions (e.g., skarns), lower Zn concentrations in clinopyroxene (Henry's law range <1500 ppm) are noted and increasing Zn content correlates with increasing metamorphic temperature conditions. Additionally, there is obviously a negative correlation between petedunnite component in clinopyroxene and the f_{S_2}/f_{O_2} ratio during formation. Thus, Zn turns out to be a key element in clinopyroxene geochemistry. It can be easily measured with high precision by electron microprobe analysis. Therefore, routine measurement of zinc in element analyses of clinopyroxenes is strongly recommended.

ACKNOWLEDGMENTS

The authors thank G. Grundmann, Technische Universität, München, F. Mädler Bayrische Staatssammlung für Geologie, München, and G. Brey, Johann Wolfgang Goethe-Universität, Frankfurt/Main, for generously supplying samples, and H. Hofstetter for preparing microprobe samples. We thank M. Huber for taking the SEM photograph of petedunnite and M. Heuer for XRD refinement of petedunnite. We also express our gratitude to E. Essene, E. Ghent, G. Amthauer, and W. Minarik for their useful reviews that strongly improved the manuscript. This research was supported by Deutsche Forschungsgemeinschaft (DFG) Grant Fe 235/5 within the priority program "Experimentelle Studien über Elementverteilung" and by Ludwig-Maximilians-University (LMU) grant, within the promotion program of gender equality.

REFERENCES CITED

Allen, R.F., Lundstrom, I., Ripa, M., and Christofferson, H. (1996) Facies analysis of a 1.9 Ga, continental margin, back-arc, felsic caldera province with diverse Zn-Pb-Ag-(Cu-Au) sulfide and Fe oxide deposits, Bergslagen region, Sweden.

Economic Geology and the Bulletin of the Society of Economic Geologists, 91, 979–1008.
Alexander, L. and Klug, H.P. (1948) Basic aspects of X-ray absorption in quantitative diffraction analysis of powder mixtures. Analytical Chemistry, 20, 886–889.
Andersson, U.B., Högdahl, K., Sjöström, H., and Bergman, S. (2006) Multistage growth and reworking of the Palaeoproterozoic crust in the Bergslagen area, southern Sweden: evidence from U-Pb geochronology. Geological Magazine, 143, 679–697.
Arlt, T. and Angel, R.J. (2000) Displacive phase transitions in C-centered clinopyroxenes; spodumene, $LiScSi_2O_6$ and $ZnSiO_3$. Physics and Chemistry of Minerals, 27, 719–731.
Billström, K. (1991) Sulphur isotope compositions in the Åmmeberg Zn-Pb ore deposit, south-central Sweden: genetic implications. Geologische Rundschau, 80, 717–727.
Birch, F. and LeComte, P. (1960) Temperature–pressure plane for albite composition. American Journal of Science, 258, 209–217.
Blum, K. (1982) Instrumentelle Neutronenaktivierung zum Studium der Elementverteilung in den Mineralphasen von Mantelgesteinen, 172 p. Ph.D. thesis, University of Mainz.
Bucher, K. and Frey, M. (1994a) Petrogenesis of Metamorphic Rocks, Chapter 4: Metamorphic grade, p. 129–132. Springer-Verlag, Berlin.
——— (1994b) Petrogenesis of Metamorphic Rocks, Chapter 9: Metamorphism of mafic rocks, p. 286–293. Springer-Verlag, Berlin.
Chatterjee, N.D. (1991) Applied Mineralogical Thermodynamics Chapter 5: Phase relations among end-member solids and fluid, p. 107–140. Springer-Verlag, Berlin.
Core, D.P., Kesler, S.E., Essene, E.J., Dufresne, E.B., Clarke, R., Arms, D.A., Walko, D., and Rivers, M.L. (2005) Copper and zinc in silicate and oxide minerals in igneous rocks from the Bingham—Park City Belt, Utah: Synchrotron X-ray-fluorescence data. The Canadian Mineralogist, 43, 1781–1796.
Doroshev, A.M., Olesch, M., Logvinov, V.M., and Malinovsky, I.J. (1983) High pressure stability of zinc clinopyroxene $ZnSiO_3$ and the occurrence of a new polytype of zinc orthosilicate Zn_2SiO_4 as a breakdown product. Neues Jahrbuch für Mineralogie, Monatshefte, 6, 277–288.
Essene, E.J. and Peacor, D.R. (1987) Petedunnite ($CaZnSi_2O_6$), A new zinc clinopyroxene from Franklin, New Jersey, and phase equilibria for zincian pyroxenes. American Mineralogist, 72, 157–166.
Ettler, V., Legendre, O., Bodénan, F., and Touray, J.-C. (2001) Primary phases and natural weathering of old lead-zinc-pyrometallurgical slag from Pøíbram, Czech Republic. The Canadian Mineralogist, 39, 873–888.
Evans, A.M. (1993) Ore Geology and Industrial Materials, p. 89–92. Blackwell Publishing, Oxford.
Fehr, K.T. (1992) Petrogenetische Teilnetze für Niedertemperatur-Hochdruck (LT-HP) Metamorphite im System Ca-Al-Fe^{3+}-Ti-Si-OH, 211 p. Habilitaion Dissertation, Ludwig-Maximilians-University of Munich.
Fehr, K.T. and Huber, A.L. (2001) Stability and phase relations of $Ca[ZnSi_3]O_8$, a new phase with feldspar structure in the system CaO-ZnO-SiO_2. American Mineralogist, 86, 21–28.
Ferry, J.W., Wing, B.A. Penniston-Dorland, S.S., and Rumble, D.I. (2002) The direction of fluid flow during contact metamorphism of siliceous carbonate rocks; new data for the Monzoni and Predazzo aureoles, northern Italy, and a global review. Contributions to Mineralogy and Petrology, 142, 679–699.
Förstner, U. and Hirschmann, G. (1997) Final research report—Long term landfill behavior of municipal solid waste incineration bottom ash, 202 p. Technical University Hamburg-Harburg, German Ministry for Education, Science Research and Technology (BMBF), Bonn; presented at Umweltbundesamt (UBA), Berlin.
Frondel, C. and Ito, J. (1966) Zincian aegirine-augite and jeffersonite from Franklin, New Jersey. American Mineralogist, 51, 1388–1393.
Frost, B.R., Frost, C.D., Hulsebosch, T.P., and Swapp, S.M. (2000) Origin of the charnockites of the Louis Lake Batholith, Wind River Range, Wyoming. Journal of Petrology, 41, 1759–1776.
Galilaeer, L. (1967) Zur Geologie und Petrographie der Skarnlager von Breitenbrunn. Deutsche Gesellschaft für Geologische Wissenschaft, Berichte, Reihe B, 12, 316–317.
Haussühl, S. and Liebertz, J. (2004) Elastic and thermoeleastic properties of synthetic $CaMgSi_2O_7$ (åkermanite) and $CaZnSi_2O_7$ (hardystonite). Physics and Chemistry of Minerals, 31, 565–567.
Heuer, M., Bente, K., and Fehr, K.T. (1996) Intrakristalline Zn-Fe –Verteilung in Hedenbergit. mittels Röntgenbeugungsdaten. Beiheft zum. European Journal of Mineralogy, 8, 105.
Heuer, M., Huber, A.L., and Bromiley, G.D. (2002a) Crystal structure of calcium iron zinc *catena*-disilicate, $Ca(Fe0_{0.52}Zn_{0.48})Si_2O_6$. Zeitschrift für Kristallographie, New Crystal Structures, 217, 465.
Heuer, M., Huber, A.L., and Redhammer, G.J. (2002b) Crystal structure of calcium iron zinc *catena*-disilicate, $Ca(Fe0_{0.19}Zn_{0.81})Si_2O_6$. Zeitschrift für Kristallographie, New Crystal Structures, 217, 467.
Heuer, M., Huber, A.L., Bromiley, G.D., Fehr, K.T., and Bente, K. (2005) Characterization of synthetic hedenbergite ($CaFeSi_2O_6$)–petedunnite ($CaZnSi_2O_6$) solid solution series by X-ray single crystal diffraction. Physics and Chemistry of Minerals, 32, 552–563.
Heuss-Aßbichler, S. and Fehr, K.T. (1994) The trace-element content of Zn in garnet, clinopyroxene and epidote as a petrogenetic indicator. Terra Abstract 1, Terra Nova, 6, 23.
Holtstam, D. and Mansfeld, J. (2001) Origin of a carbonate-hosted Fe-Mn-(Ba-As-Pb-Sb-W) deposit of Långban-Type in central Sweden. Mineralium Deposita, 36, 641–657.
Huber, A.L. and Fehr K.T. (2002) Crystal chemistry and thermodynamic mixing properties of hedenbergite-petedunnite-johannsenite-diopside solid solutions. EMPG IX, Ninth International Symposium on Experimental Mineralogy, Petrology and Geochemistry, Journal of Conference Abstracts, 7, 47.
——— (2003) Thermodynamische Eigenschaften der Mischreihe Hedenbergit-Petedunnit $Ca(Fe,Zn)Si_2O_6$. Mitteilungen der Österreichischen Mineralogischen Gesellschaft, 48, 172–173.
Huber, A.L. Heuer, M., Fehr, K.T., Bente, K., Schmidbauer, E., and Bromiley, G.D. (2004) Characterization of synthetic hedenbergite ($CaFeSi_2O_6$)—petedunnite ($CaZnSi_2O_6$) solid solution series by X-ray powder diffraction and ^{57}Fe Moessbauer spectroscopy. Physics and Chemistry of Minerals, 31, 67–79.
Huckenholz, H.G., Lindhuber, W., and Springer, J. (1974) The join $CaSiO_3$-Al_2O_3 of the CaO-Al_2O_3-Fe_2O_3-SiO_2 quaternary system and its bearing on the formation of granditic garnets and fassaitic pyroxenes. Neues Jahrbuch für Mineralogie, Abhandlungen, 121, 160–207.
Huckenholz, H.G., Hölzl, E., and Lindhuber, W. (1975) Grossularite, its solidus and liquidus relations in the CaO-Al_2O_3-SiO_2-H_2O system up to 10 kbar. Neues Jahrbuch für Mineralogie, Abhandlungen, 124, 1–46.
Jahanbagloo, I.C. and Zoltai, T. (1968) Quantitative analysis with the aid of calculated X-ray powder patterns. Analytical Chemistry, 40, 1739–1741.
Johnson, C.A. and Skinner, B.J. (2003) Geochemistry of the Furnace Magnetite Bed, Franklin, New Jersey and the relationship between stratiform iron oxide ores and stratiform zinc oxide-silicate ores in the New Jersey Highlands. Economic Geology, 98, 837–854.
Jonsson, E. and Broman, C. (2002) Fluid inclusions in the late-stage Pb-Mn-As-Sb mineral assemblages in the Långban deposit, Bergslagen, Sweden. The Canadian Mineralogist, 40, 47–65.
Klug, H.P. and Alexander, L. (1974) X-ray Diffraction Procedures for Polycrystalline and Amorphous Materials, Chapter 7-2: Quantitative analysis of powder mixtures, p. 531–536. Wiley, New York.
Klug, H.P., Alexander, L., and Kummer, E. (1948) Quantitative analysis with the X-ray spectrometer. Accuracy and reproducibility. Analytical Chemistry, 20, 607–609.
Kumpulainen, R.A., Mansfeld, J., Sundblad, K., Neymark, L., and Bergman, T. (1996) Stratigraphy, age, and Sm-Nd isotope systematics of the country rocks to Zn-Pb sulfide deposits, Åmmeberg District, Sweden. Economic Geology, 91, 1009–1021.
Lottermoser, B.G. (2002) Mobilization of heavy metals from historical smelting slag dumps, north Queensland, Australia. Mineralogical Magazine, 66, 475–490.
Mirwald, P.W. and Massonne, H.J. (1980) The low-high quartz and quartz-coesite transition up to 40 kbar between 600 and 1600 °C and some reconnaissance data on the effect of Na_2O on the low-quartz-coesite transition. Journal of Geophysical Research, B, 85, 12, 6983–6990.
Morimoto, N., Nakajima, Y., Syono, Y., Akimoto, S., and Matsui, Y. (1975) Crystal structures of pyroxene-type $ZnSiO_3$ and $ZnMgSi_2O_6$. Acta Crystallographica, B31, 1041–1049.
Nakano, T. (1998) Pyroxene geochemistry as an indicator for skarn metallogenesis in Japan. In D.R. Lentz, Ed., Mineralized intrusion—related skarn systems, 26, p. 147–167. Mineralogical Association of Canada Short course series, Québec.
Nakano, T., Yoshino, T., and Nishida, N. (1991) Rapid analytical method for trace Zn contents in some mafic minerals using the electron microprobe: Potential utility as a metallogenetic a petrogenetic indicator. Chemical Geology, 89, 379–389.
Nakano, T., Yoshino, T., Shimazaki, H., and Shimizu, M. (1994) Pyroxene composition as an indicator in the classification of skarn deposits. Economic Geology, 89, 1567–1580.
Nestola, F., Boffa Ballaran, T., Angel, R.J., Zhao, J., and Ohashi, H. (2010) High-pressure behavior of Ca/Na clinopyroxenes: The effect of divalent and trivalent 3d-transition elements. American Mineralogist, 95, 832–838.
Newton, M.S. and Kennedy, G.C. (1968) Jadeite, analcite, nepheline and albite at high temperatures and pressures. American Journal of Sciences, 266, 728–735.
Newton, M.S. and Smith, J.V. (1967) Instigations concerning the breakdown of albite at depth in the earth. Journal of Geology, 75, 268–286.
Ohashi, H., Osawa, T., Sato, A., and Tsukimura, K. (1996) Crystal structures of (Na, Ca)(Sc,Zn)Si_2O_6 clinopyroxenes formed at 6 GPa. Journal of Mineralogy, Petrology and Economic Geology, 91, 21–27.
Olesch, M., Doroshev, A.M., and Nekhaev, P.Y. (1982) Low pressure stability of zinc clinopyroxene ($ZnSiO_3$). Neues Jahrbuch für Mineralogie, Monatshefte, 312–320.
Olmi, F., Viti, C., Bindi, L., Bonazzi, P., and Menchetti, S. (2000) Second occurrence

of okayamalite, $Ca_2SiB_2O_7$: Chemical and TEM characterization. American Mineralogist, 85, 1508–1511.
Peck, W.H., Volkert, R.F., Meredith, M.T., and Rader, E.L. (2006) Calcite-graphite thermometry of the Franklin marble, New Jersey Highlands. The Journal of Geology, 114, 485–499.
Peng, Q. and Bromley, A.V. (1992) Fluid inclusion studies in the skarn-type tin mineralization at Red-A-ven, Northwest Dartmoor, England. Chinese Journal of Geochemistry, 11, 362–369.
Popp, R.K. and Gilbert, M.C. (1972) Stability of acmite-jadeite pyroxenes at low pressure. American Mineralogist, 57, 1210–1231.
Pouchou, L. and Pichoir, F. (1984) A new model for quantitative X-ray microanalysis. Part I: Application to the analysis of homogeneous samples. Recherche Aerospatiale, 3, 13–38.
Proyer, A. (2003) Metamorphism of pelites in NKFMASH—a new petrogenetic grid with implications for the preservation of high pressure mineral assemblage during exhumation. Journal of Metamorphic Geology, 21, 493–509.
Puziewicz, J., Zainoun, K., and Bril, H. (2007) Primary phases in pyrometallurgical slags from a zinc-smelting waste dump, Świętochłowice, Upper Silesia, Poland. The Canadian Mineralogist, 45, 1189–1200.
Rothkopf, A., Fehr, K.T., and Heuer, M. (1998) Stabilitäts- und Phasenbeziehungen von $CaZnSi_3O_8$-einer neuen Phase mit Feldspatstruktur im System CaO-ZnO-SiO_2. Beiheft zum European Journal of Mineralogy, 10, 243.
Segnit, E.R. (1954) The system CaO-ZnO-SiO_2. Journal of the American Ceramic Society, 37, 273–277.
Sepp, B. (1998) Ti-Einbau in Pyroxenen—experimentelle Untersuchungen in den Systemen CaO-MgO-Al_2O_3-SiO_2-TiO_2 und CaO-MgO-SiO_2-TiO_2, 181 p. Ph.D. thesis, Ludwig-Maximilians-University of Munich.
Shimizu, M. and Iiyama, J.T. (1982) Zinc-Lead Skarn Deposits of he Nakatatsu Mine, Central Japan. Economic Geology, 77, 1000–1012.
Sonnet, P.M. and Verkaeren, J. (1989) Scheelite—malayite and axinite-bearing skarns from El Hammam, Central Morocco. Economic Geology, 84, 575–590.
Suryanarayanan, R. (1989) Determination of the relative amounts of anhydrous carbamazepine ($C_{15}H_{12}N_2O$) and carbamazepine dihydrate ($C_{15}H_{12}N_2O{\cdot}2H_2O$) in a mixture by powder X-ray diffractometry. Pharmaceutical Research, 6, 1017–1024.
Volkert, R.A. (2001) Geologic setting of Proterozoic iron, zinc and graphite deposits, New Jersey Highlands. In J.F. Slack, Ed., Geologic setting of Proterozoic iron, zinc, and graphite deposits, New Jersey Highlands. Guidebook Series, 35, p. 59–73. Society of Economic Geologists, Littleton, Colorado.
Wagner, T., Jonsson, E., and Boyce, A.J. (2005) Metamorphic ore remobilization in the Hällefors district, Bergslagen, Sweden: constraints from mineralogical and small-scale sulphur isotope studies. Mineralium Deposita, 40, 100–114.
Wesolowski, D. and Ohmoto, H. (1988) Remobilization of molybdenum from W-Mo skarns by late meteoric fluids at King Island, Tasmania. Abstracts with Programs—Geological Society of America, 13, 578.
White, G.K. and Roberts, R.B. (1988) Thermal expansion of willemite Zn_2SiO_4. Australian Journal of Physics, 41, 791–795.
Yoder, H.S. (1950) High-low quartz inversion up to 10,000 bars. Transactions, American Geophysical Union, 31, 827–835.
Yu, S. and Smith, D.K. (1983) Crystal structure of a Na-augite from San Carlos, northern Arizona. Chung Kuo Ti Ch'ih Hsueh Hui ChuanKan. Memoir of the Geological Society of China, 5, 147–166.

Manuscript received March 22, 2011
Manuscript accepted January 2, 2012
Manuscript handled by Edward Ghent